Self-Organized Criticality and the Barkhausen Effect

P. J. Cote and L. V. Meisel
Benet Laboratories, Watervliet Arsenal, Watervliet, New York 12189
(Received 12 April 1991)

The Barkhausen effect was studied in an amorphous alloy. The data exhibit all the attributes of self-organized critical behavior enumerated by Bak, Tang, and Wiesenfeld: The distribution of lifetimes and areas of discrete Barkhausen pulses follow power-law distributions, which have been modified to account for finite-size effects as suggested by Kadanoff, Nagel, Wu, and Zhou. The directly measured power spectral density has the form of flicker noise, with exponent and form consistent with those to be expected from the measured distribution of pulse areas and lifetimes in the light of the work of Jensen, Christensen, and Fogedby.

PACS numbers: 75.60.Ej

The theory of self-organized criticality (SOC) introduced by Bak, Tang, and Wiesenfeld [1] (BTW) provides a description of the dynamics of spatially extended dissipative systems. The principal conclusion of BTW is that dissipative dynamical systems tend to organize themselves into a critical state where chain reactions of *all* sizes in time and space propagate through the system.

The absence of characteristic length and time scales in the self-organized critical state of large dissipative dynamical systems has important consequences: fractal structure and a "$1/f$" noise power spectral density. Thus, SOC provides a unified, coherent explanation for the routine observation of $1/f$ noise and fractal structure in nature. A collateral consequence of SOC is power-law dependences of numbers of occurrences on energies released, chain-reaction lifetimes, and cluster sizes.

A subsequent paper by Jensen, Christensen, and Fogedby [2] (JCF) clarified the underlying ideas in BTW and made explicit the important connection between the power-law dependences and the power spectral densities suggested by BTW. Kadanoff, Nagel, Wu, and Zhou [3] extended the theory to apply to SOC phenomena occurring in systems of (spatially) finite extent.

SOC has been the focus of many recent investigations. For example, computer simulations and laboratory experiments on sandpile dynamics [4], coarsening of cellular magnetic domain patterns in garnet films [5], and models of domain pattern development on magnetic tape [6] show "fingerprints" of SOC. The most spectacular example of the power-law characteristic of SOC is the Gutenberg-Richter law for the distribution of earthquake magnitudes [7].

The physics of the Barkhausen effect make it a good candidate for description in terms of self-organized criticality. The magnetic characteristics of a ferromagnet are determined by its magnetic domain distribution and the response of these domains to applied magnetic fields. For small fields, the kinetic barriers permit only small, reversible, domain-wall changes and the system remains magnetically elastic. As the applied field increases and approaches the magnitude of the coercive force, the specimen magnetization increases very rapidly and the response is characterized by large and irreversible domain-wall jumps along with magnetization rotations within domains. At saturation, the entire specimen is magnetized in the direction of the applied field. The intermittent changes in magnetization that characterize the Barkhausen effect are detected as voltage pulses in a pickup coil near the specimen. The stochastic nature of the domain responses arises from the complicated character of local fields, internal stresses, and bulk and surface defects. Barkhausen rearrangements tend to occur as clusters of domain-wall jumps comprising a chain reaction initiating at a single domain. Thus, many characteristic features of the vertical portion of a magnetic hysteresis loop are similar to those seen in model simulations of the self-organized critical state.

Support for this description may be found in the Barkhausen-effect literature. The coarsening of cellular magnetic domains in garnet films [5], which has been interpreted in terms of SOC, can be viewed as a special case of more general Barkhausen phenomena. Furthermore, spectrum analyses of Barkhausen noise generally show $1/f$ dependence that is thought to be a key indicator of SOC. (Various alternative explanations [8] for this behavior have been presented.) The present study is directed at examining the fingerprints of SOC in the Barkhausen effect in a ferromagnetic metallic glass and tests whether a consistent description of the phenomena is possible in the light of Refs. [1–3].

Ferromagnetic amorphous alloys are well suited to a search for SOC in Barkhausen noise: The high resistivity of amorphous phases significantly lowers eddy-current damping of domain-wall motion. Hysteresis loops are rectangular, so that Barkhausen noise originates in regions of essentially constant, high permeability. Furthermore, their coercive force is small (≈ 0.1 Oe), so that samples may be cycled through the hysteresis loop with small external fields.

The particular alloy selected for study was Metglas 2605S-2 ribbon supplied by Allied-Signal, which has the additional advantage that its domain structures have been

described by Livingston and Morris [9]. The domains are distributed as a fine network of complex patterns in unmagnetized specimens in the as-cast state, while the domains can be large (of the order of sample dimensions) following annealing.

Barkhausen data were obtained from as-cast and annealed samples. The magnetic annealing involved heating to 400 °C and immediately cooling at rates of 25 °C/min in a field of 120 Oe. Sample widths were 5 mm for as-cast specimens and 1 mm for annealed samples; lengths ranged from 2 to 4 cm; and the thickness was nominally 25 μm but varied by 30%, due to nonuniformities in the casting process. Narrower specimens were employed to compensate for the smaller amplitude of Barkhausen pulses, which is a consequence of permeability and eddy-current-damping effects in magnetically annealed alloys.

A 300-turn pickup coil was wrapped closely around the central region of the ribbons. A Pacific Instruments preamplifier was used with a factor-of-1000 amplification. The driving field for the as-cast specimen was provided by a rotating permanent magnet in the proximity of the specimen. For the annealed case, the specimen and its pickup coil were placed inside an air-core solenoid with the long axis of the specimen aligned parallel to the alternating field. There was no detectable difference in pulse trains with the two methods. The field was varied slowly (1 Oe/s) to maintain separation of individual Barkhausen events. Trains of Barkhausen pulses were recorded in a random fashion on a Nicolet digital storage scope from which the time duration and integrated areas of individual events were obtained.

Barkhausen noise pulses, typical of those obtained in the present study, are shown in Fig. 1. The pulses are generally comprised of a chain of individual events manifested as multiple peaks within a pulse. The observed pulse shapes differ from the rectangular forms assumed in the JCF analysis; however, the associated single-pulse autocorrelation functions may be reasonably approximated

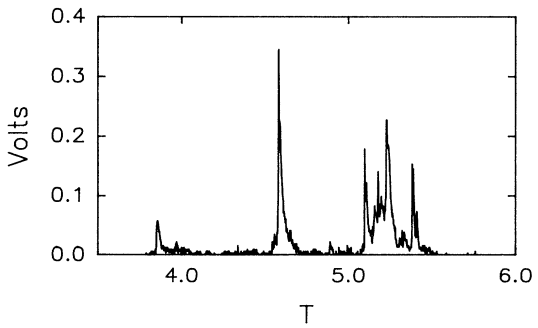

FIG. 1. Typical Barkhausen pulses observed in a 5-mm-wide as-cast ribbon of Metglas 2605S-2. There are three relatively large events comprised of clusters of pulses which are well separated by many smaller events. The small pulses can be difficult to distinguish from the background. Time units are milliseconds.

by the triangular JCF autocorrelation function shape. There is clear separation of the major pulses. Pulse durations and areas were obtained from random selections of typically 5-ms trains of such pulses; direct measures of the power spectral density were obtained from typically 40-ms trains of such pulses.

Large errors are inherent in the measurement of the distribution of lifetimes for low-intensity, short-duration pulses, since the large number of small pulses eventually blend into a low-level background noise. Thus, pulses having lifetimes T less than 50 μs were not included in the present analysis. Employing this criterion, a maximum of 2763 (1324) pulses were selected for analysis in the as-cast (magnetically annealed) samples. The data were organized into 20-bin linearly spaced histograms. We varied the minimum T between 50 and 90 μs in order to provide an estimate of the uncertainties in the deduced fitting parameters. The occupation of the bin centered at T is denoted $N(T)$. The intrinsic distribution of lifetimes $P(T)$ in the Barkhausen noise is assumed to be proportional to the measured $N(T)$.

Employing the Nelder-Mead downhill simplex algorithm [10] to minimize the square deviations in $N(T)$, the data were fitted by the form

$$P(T) \propto T^a \exp(-T/T_0), \quad N(T) \propto P(T), \tag{1}$$

where a and T_0 are constants. As the minimum T was varied between 50 and 90 μs, the fit parameter a varied between -1.83 and -2.61 (-1.98 and -2.60) and T_0 varied between 351 and 1274 μs (420 and 1074 μs) in the as-cast (annealed) samples. (For a few values of the minimum T, best fits were pure power-law forms with $a \approx 3.0$; these values were not included above or in the determinations of mean values, etc.) The parameters were strongly correlated (larger magnitude of a occurring with larger T_0) and $a = -2.26 \pm 0.35$ (-2.37 ± 0.30), $\langle T_0 \rangle \equiv \exp[\text{mean}\{\ln(T_0)\}] = 844$ μs (730 μs) in as-cast (annealed) samples. A typical plot of $N(T)$ vs T and the fit curve are shown in Fig. 2.

The form in Eq. (1) is compatible with the JCF analysis. A physical interpretation for the exponential term with constant T_0 can be found in the finite-size scaling discussion of Kadanoff, Nagel, Wu, and Zhou [3]. The parameter T_0, which is of the order of the maximum pulse length observed for a given specimen, may be interpreted in terms of the size-effect SOC model. The agreement of the parameters in the as-cast and narrower annealed specimens indicates that the size effect is determined by defect distributions rather than by macroscopic physical boundaries as in sandpile experiments [4] and simulations [1,3].

In order to compute the distribution of weighted lifetimes, $G(T)$, as defined by JCF, it is necessary to determine the joint probability of pulses of lifetime T and area A, $P(A,T)$, which can be expanded in the form $P(A,T) = P(T)P(A|T)$, where $P(A|T)$ is the condition-

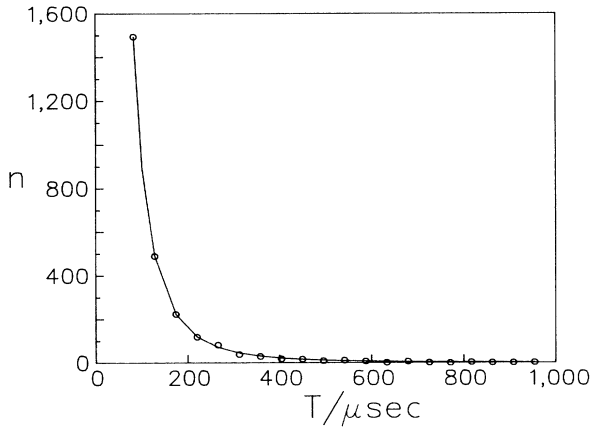

FIG. 2. Plot of measured distribution of Barkhausen pulse lifetimes T for $T > 59$ μs in as-cast ribbon. The curve is the result of least-squares fitting of the data by Eq. (1); the fitting parameters are $a = -2.36$ and $T_0 = 611$ μs.

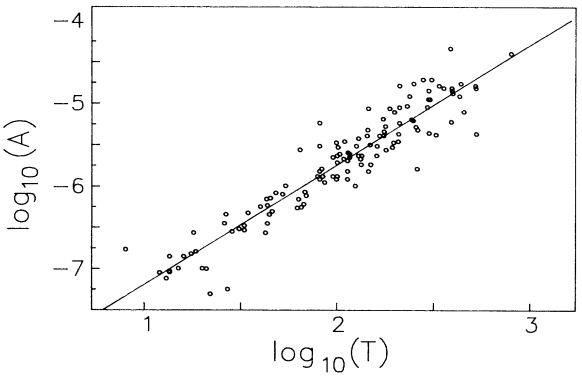

FIG. 3. Log-log plot of 125 samplings of pulse area A (in Vs) vs pulse duration T (in μs) in as-cast ribbon. The straight line is a least-squares fit to the data.

al probability for a pulse of lifetime T to have area A. Figure 3 is a log-log plot of pulse area A versus lifetime T for a "random" selection of pulses of various lifetimes for the as-cast sample. Similar plots were obtained for annealed specimens. In principle, such data could be used to precisely determine the conditional probability $P(A|T)$; however, to compute the parameters in the JCF expression for $G(T)$, we take $P(A|T) \approx \delta(A - A_1 T^g)$ with $g = 1.45$ (1.34) for the as-cast (annealed) case from least-squares fitting by

$$A(T) \propto T^g . \tag{2}$$

The distribution of weighted lifetimes $G(T)$, as defined by JCF, is then determined as follows:

$$G(T) = \int_0^\infty dA\, P(A,T)[A/T]^2$$
$$= P(T) \int_0^\infty dA\, P(A|T)[A/T]^2 \propto P(T) T^{2(g-1)} \propto N(T) T^{2(g-1)} \propto T^{2(g-1)+a} \exp(-T/T_0) . \tag{3}$$

The parameters a and T_0 in the JCF expression,

$$G(T) \propto T^a \exp(-T/T_0) , \tag{4}$$

can then be evaluated, yielding $a = 2(g-1)+a \approx -1.59$ (-1.46) for the as-cast (annealed) case.

According to the JCF analysis, the parameters a and T_0 in $G(T)$ determine the form of the power spectral density:

$$S(f) \propto (1/f)^E \text{ for } f > 1/T_0 , \tag{5a}$$

where

$$E = \begin{cases} 3+a \text{ for } a < -1, \\ 2 \text{ for } a \geq -1 , \end{cases}$$

and

$$S(f) = \text{const for } f < 1/T_0 . \tag{5b}$$

Hence, the JCF analysis yields a $1/f$ noise spectrum, modified by finite-size effects [3], with $E = 1.41$ (1.54), with a transition to an f-independent form below 1185 Hz (1370 Hz) for the as-cast (annealed) samples.

We can also determine $S(f)$ directly from autocorrelation functions measured for trains of Barkhausen pulses. Figure 4 is a log-log plot of the power spectral density $S(f)$, obtained by Fourier transformation of the autocorrelation function (Nyquist theorem) determined directly (from the digitized output) from a train of about 40 ms, versus frequency f for an annealed sample. The jagged curve includes every tenth point of ten-point-running averaged data. The data are averaged to smooth out the large fluctuations that characterize discrete numeric Fourier transforms of such data.

Least-squares fitting of the data in Fig. 4 by the form in Eq. (5) for $f > 2$ kHz yields $E = 1.244$. The data in Fig. 4 become frequency independent below about 1000 Hz; similar data were obtained for an as-cast specimen. Results for fifteen least-squares fits for minimum f ranging from 1 to 20 kHz yielded $E = 1.11 \pm 0.05$ (1.26 ± 0.07) for as-cast (annealed) specimens.

Some specimens exhibited several large pulses which were closely related to the magnitude of the external field rather than randomly distributed as expected in SOC. Examination of domain-wall motion in these specimens using the Bitter powder method with a ferrofluid showed corresponding repetitive domain jumps adjacent to cut edges. We believe that these pulses are produced by the breaking free of strongly pinned domains and are not representative of the bulk of domain jumps.

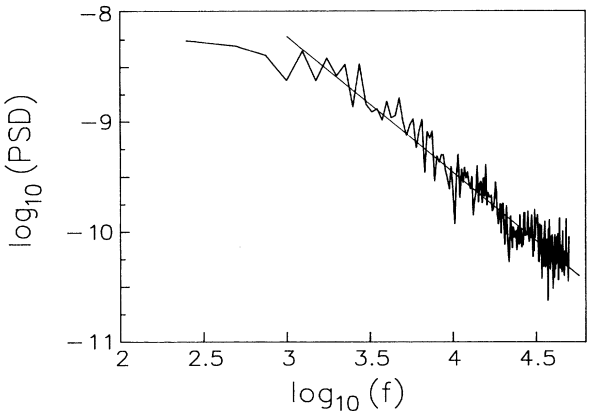

FIG. 4. Log-log plot of every tenth value of the power spectral density (in V^2s^2) averaged over ten values (obtained via discrete Fourier transform) vs frequency (in Hz) of a 40-ms train in magnetically annealed ribbon. The straight line, which is least-squares fit for $f > 2$ kHz, has a slope of -1.244.

The Barkhausen effect in magnetically annealed and as-cast specimens of Metglas 2605S-2 ribbon exhibits all the attributes of SOC behavior enumerated by Bak, Tang, and Wiesenfeld [1]: The weighted distribution of discrete Barkhausen pulse lifetimes follows a power-law distribution, modified to account for finite-size effects as suggested by Kadanoff, Nagel, Wu, and Zhou [3]. The directly measured power spectral density has the form of flicker noise, with exponent and form consistent with those to be expected from the weighted distribution of pulse lifetimes in light of the work of Jensen, Christensen, and Fogedby [2].

We wish to thank Raymond D. Scanlon and Tammy Hickey for advice and assistance.

[1] P. Bak, C. Tang, and K. Wiesenfeld, Phys. Rev. Lett. **59**, 381 (1987); Phys. Rev. A **38**, 36 (1988).
[2] H. J. Jensen, K. C. Christensen, and H. C. Fogedby, Phys. Rev. B **40**, 7425 (1989).
[3] L. P. Kadanoff, S. R. Nagel, L. Wu, and S-M. Zhou, Phys. Rev. A **39**, 6524 (1989).
[4] G. A. Held, D. H. Solina, II, D. T. Keane, W. J. Hagg, P. M. Horn, and G. Grinstein, Phys. Rev. Lett. **65**, 1120 (1990).
[5] K. L. Babcock and R. M. Westervelt, Phys. Rev. Lett. **64**, 2168 (1990).
[6] X. Che and H. Suhl, Phys. Rev. Lett. **64**, 1670 (1990).
[7] B. Gutenberg and C. F. Richter, Ann. Geofis. **9**, 1 (1956).
[8] See, for example, B. Alessandro, C. Beatrice, G. Bertotti, and A. Montorsi, J. Appl. Phys. **68**, 2908 (1990); and H. Bittel, IEEE Trans. Magn. **5**, 359 (1969).
[9] J. D. Livingston and W. G. Morris, J. Appl. Phys. **57**, 3555 (1985).
[10] See, for example, the subroutine AMOEBA, in William H. Press, Brian P. Flannery, Saul A. Teukolsky, and William T. Vetterling, *Numerical Recipes* (Cambridge Univ. Press, Cambridge, 1986).